SIAM J. SCI. COMPUT.
Vol. 35, No. 6, pp. B1285–B1303

COUPLING REMESHED PARTICLE AND PHASE FIELD METHODS FOR THE SIMULATION OF REACTION-DIFFUSION ON THE SURFACE AND THE INTERIOR OF DEFORMING GEOMETRIES*

GERARDO TAURIELLO† AND PETROS KOUMOUTSAKOS†

Abstract. Reaction-diffusion systems on the surface and the interior of complex domains are potent models of growth in living organisms. The simulation of these models requires numerical methods capable of handling large deformations and the accurate coupling of the evolution of substances in the lumen and on the surface of the deforming geometries. Here, we develop a novel computational method to handle such problems by combining a remeshed particle method with a phase field method. Remeshed particle methods are well suited to discretizing deforming geometries, while the phase field method is used to impose boundary conditions that effectuate the coupling of substances evolving in their lumen and on their surfaces. We demonstrate that this hybrid method enables for the first time the accurate coupling of reaction-diffusion on a deformable surface and its interior. The method is validated on benchmark problems and the the effect of lumen diffusion to a pattern forming reaction-diffusion system on a deforming surface is discussed.

Key words. Laplace–Beltrami operator, advection-reaction-diffusion equation, deforming surfaces, particle method, level set method, phase field method

AMS subject classifications. 92C15, 35Q92, 35K57, 35R35, 76M28

DOI. 10.1137/130906441

1. Introduction.

Reaction-diffusion systems are classic models of essential biological processes such as organogenesis and tumor and plant growth [49, 50]. The majority of reaction-diffusion models is concerned with the evolution of either volume or surface bound substances. The additional complexity of substances synchronously evolving in three dimensions, on deforming surfaces, and in their interior presents a number of challenges to numerical methods. We address these challenges by coupling remeshed particles and phase field methods.

Simulations in nondeforming, two-dimensional (2D) domains of activator-inhibitor and activator-substrate systems give rise to spots and stripes and other patterns encountered in nature [39, 21, 3]. Varea, Aragon, and Barrio considered pattern formation on the surface of a sphere, using a linearized Brusselator [51]. In turn, Chaplain, Ganesh, and Graham proposed the Schnakenberg system as a patterning mechanism on the surface of spherical tumors [9]. They suggest that the generated spots could act as a prepattern that would then lead to exophytic growth of the tumor and invasion into the surrounding tissue. Madzvamuse and Maini studied the effect of continuously growing 2D domains on the formed patterns [33]. In recent years, reaction-diffusion systems have been coupled with models of active transport and mechanical signaling to understand pattern formation [23, 18]. Baker and Maini used a reaction-diffusion system to model the morphogen Dpp in a one-dimensional (1D) representation of the developing Drosophila wing disc [2]. More recently, Soriano et al. proposed a coupling between mechanical stress and a 1D activator-inhibitor system to regulate symmetry breaking in the regeneration of hydra [47].

*Submitted to the journal's Computational Methods in Science and Engineering section January 18, 2013; accepted for publication (in revised form) September 16, 2013; published electronically December 3, 2013. This work was supported by the SystemsX.ch initiative within the framework of the WingX project.

http://www.siam.org/journals/sisc/35-6/90644.html

†Computational Science and Engineering Laboratory, ETH Zurich, CH-8092 Zurich (gtauriello@inf.ethz.ch, petros@ethz.ch).

1.1. Diffusion on deforming surfaces and in the interior. Holloway and Harrison proposed an extended version of the Brusselator reaction-diffusion model for pattern selection in plants [16]. The system is solved on the surface of a hemisphere that deforms in time according to the concentration of one of the species. The surface is discretized as a triangle mesh and the system is solved using a finite element model (FEM) [53]. The explicit representation of the surface, via triangulation, allows for the efficient solution of the reaction-diffusion equation. However, when the surface is deformed, the finite elements can become distorted leading to numerical artifacts and requiring retriangulation of the surface.

Level sets use an implicit representation to capture accurately smooth surfaces and their deformations [37, 45, 36]. Bertalmio et al. introduced a level set method to perform diffusion calculations on implicit surfaces [7]. The surface quantities are extended into a narrow band around the surface and the Laplace–Beltrami operator is then discretized on a regular lattice within the narrow band. This formulation was used to compute the transport and diffusion of quantities on deforming surfaces [1, 52]. Second order convergence of the discretization was shown numerically on static and moving surfaces embedded in two dimensions and three dimensions. Remeshed particle methods were also used for the simulation of reaction-diffusion processes on surfaces undergoing large deformations [6]. The closed point method was introduced as an alternative to extend surface quantities into the narrow band [43]. This method enables the use of the standard Laplace operator instead of the Laplace–Beltrami operator within the narrow band and supports open surfaces with boundaries. The work was later extended for use with implicit time stepping schemes [31].

Alternatives to level set methods in representing surfaces implicitly are phase field methods. Phase field methods have been proposed to compute diffusion inside an arbitrary volume embedded in a larger domain and discretized on a regular lattice [22]. Levine and Rappel later extended the method to allow for Robin boundary conditions on the surface [30]. They include surface quantities which are not allowed to diffuse but can locally react with other surface quantities and be transferred to and from the volume. The diffusion equation is solved using the alternating direction implicit method. Penalization methods have been proposed to enforce Dirichlet, Neumann, and Robin boundary conditions for the heat equation within irregular geometries [20, 42]. Similarly to the phase field method, the geometry is embedded within a larger domain but results have shown that a first order accuracy or less is obtained by those methods. A level set method was used to solve the Poisson and heat equations where the values are extrapolated out of the domain to enforce Robin boundary conditions [38]. A cut-cell finite volume method was developed to solve reaction-diffusion systems within arbitrary geometries which are deformed using a level set method [48]. The similar virtual node method was proposed to solve elliptic problems with immersed interfaces or within embedded boundaries. Their method cuts cells of a regular lattice and solves the system using an FEM [4]. An extended comparison of these methods is shown in Appendix A.

Novak et al. coupled reaction-diffusion systems in a stationary volume and on its surface [35]. The method was applied to evaluate errors in measurements from fluorescence loss in photobleaching experiments. They use a regular lattice to discretize the domain and a finite volume scheme to solve the equations. They use a staircase approximation of the surface which can lead to numerical errors. Voronoi meshing is used to compute the surface normals which are needed to solve diffusion on the surface and for the boundary conditions in the volume. They show convergence of the numerical solutions for the diffusion equation on a sphere and for a system

where surface and volume diffusion are coupled. Their numerical discretization of the Laplace–Beltrami operator on the surface of a sphere shows a diverging error. In a recent work, Halatek and Frey analyzed Min-protein dynamics in E. coli by solving a coupled set of reaction-diffusion equations on the surface and in the interior of a static 2D geometry using FEM [13]. To the best of our knowledge no reaction-diffusion systems have been simulated with simultaneously evolving substances in the lumen and on the surface of deforming geometries.

1.2. Remeshed particle methods for deforming surfaces. Level set and phase field methods are commonly described in an Eulerian formulation and discretized using finite difference or finite volume schemes on fixed meshes. These discretizations introduce extra dispersion or dissipation artifacts even in flows with zero velocity gradient such as solid body rotation and translation [11]. Enright et al. introduced Lagrangian marker particles at subgrid resolution to increase the accuracy of the Eulerian level set advection [11]. A recent method introduced by Leung and Zhao connects each grid point in the neighborhood of the interface, to a particle at the closest location on the interface [28]. More recently, the method was extended to solve reaction-diffusion systems on deforming surfaces using those particles [27].

Remeshed particles are an alternative method that uses particles to discretize the entire level set. It relies on the Lagrangian formulation of the level set's evolution that is handled by advecting the particles [14]. The method introduces only initialization errors, that can be easily minimized, for evolutions of solid body translation and rotation. A known problem of Lagrangian methods is the deformation of the particle locations that renders particle approximations of continuous functions inaccurate. Remeshing was introduced to resolve this problem, by projecting the weights of distorted particles on regularized particle locations while conserving the moments of the functions carried by the particles [24]. The remeshing procedure is computationally inexpensive as it only involves mapping the particle values onto a new set of particles located on a regular lattice. The method has been shown to handle accurately a wide range of problems in complex and deforming geometries [25, 26]. Recent work has shown the unique relation of remeshed particle methods with semi-Lagrangian methods and finite difference schemes [10]. Bergdorf, Sbalzarini, and Koumoutsakos later applied [6] the remeshed particle methods to the projections of Bertalmio et al. [7] to solve reaction-diffusion systems on deforming surfaces. Remeshing also enables the deployment of multiresolution particles, allowing for unprecedented accuracy in the evolution of level sets in benchmark problems [5]. Remeshed particle methods, however, encounter problems when it is necessary to impose accurate boundary conditions. This open problem is the subject of the present paper.

1.3. A coupling method of diffusion on the surface and the interior. The present work relies on the projection operator introduced by Bertalmio et al. [7] and its discretization using remeshed particle methods by Bergdorf, Sbalzarini, and Koumoutsakos [6] to handle diffusion on surfaces. The method is combined with the phase field method [30] so as to couple, for the first time, reaction-diffusion systems on the surface and in the interior of deforming geometries. We propose a formulation where the phase field is computed as a function of the level set. We choose a level set formulation as it can capture large deformations of the interface. We use a Lagrangian method to track the interface due to its increased accuracy. Specifically, we discretize and solve the advection equations with a remeshed particle method as it removes numerical dissipation without increasing the number of computational elements. The phase field method has a low computational cost and it is shown to

have second order accuracy in solving the diffusion equation. It also naturally defines the volume quantities within a narrow band around the surface. Both surface and volume quantities are defined within that band and this property is critical in order to couple the two systems. We permit boundary conditions on edges of the surface and allow the surface deformation to be confined within arbitrarily shaped geometries. We show convergence of the method on benchmark problems and compare our results with those of Holloway and Harrison [16] and Novak et al. [35]. We demonstrate our approach on a pattern-forming Schnakenberg model active in the interior and on the surface of a concentration dependent deformation of a sphere.

The outline of this article is as follows: In section 2 we present the governing equations on the surface and its interior and their extension into a shared computational domain. Section 3 describes the numerical discretization of the equations. In section 4 we show results of benchmark problems and pattern-forming reaction-diffusion systems with deforming domains. Section 5 summarizes the results and discusses strengths and weaknesses of our method.

2. Reaction-diffusion on a deforming surface and its interior. We consider N_s species that react and diffuse on a smooth closed surface $\Gamma(t)$ which can deform in time. Similarly, we have N_v species which react and diffuse inside the volume $\Omega(t)$ enclosed by $\Gamma(t) = \partial\Omega(t)$ (see Figure 2.1). The concentrations of those species will be denoted as c_s with $s = 1, \ldots, N_s$ for the surface species and as c_v with $v = N_s + 1, \ldots, N_s + N_v$ for the volume species. To simplify notation, we also introduce the vector $\mathbf{c}_s$ containing all surface species, the vector $\mathbf{c}_v$ containing all volume species, and the vector $\mathbf{c} = \mathbf{c}_s \cup \mathbf{c}_v$ containing all species. We note that $\mathbf{c}_s$ and $\mathbf{c}$ are only defined on $\Gamma(t)$ while $\mathbf{c}_v$ is defined on all of $\Omega(t)$ including its boundary $\Gamma(t)$. $\mathbf{c}$ will be used to couple surface and volume concentrations through reactions and boundary conditions for the diffusion equations.

2.1. Reaction-diffusion on a deforming surface. We consider a surface $\Gamma(t) = \{\mathbf{x}_\Gamma(t)\}$ that deforms in time according to the velocity field $\mathbf{v}_\Gamma$:

$$\frac{d\mathbf{x}_\Gamma(t)}{dt} = \mathbf{v}_\Gamma. \tag{2.1}$$

On $\Gamma(t)$, we solve equations of the form

$$\frac{\partial c_s}{\partial t} + \nabla_\Gamma \cdot (c_s \mathbf{v}_\Gamma) = D_s \Delta_\Gamma c_s + R_s(\mathbf{c}) \tag{2.2}$$

for each species s on the surface. Each species s is defined by its concentration c_s, its diffusion constant D_s, and its reaction terms $R_s(\mathbf{c})$. We note that the reaction terms can involve both surface and volume species. Δ_Γ is the Laplace–Beltrami operator on Γ expressing diffusion along the surface.

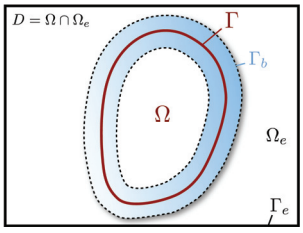

FIG. 2.1. *Extended computational domain.*

2.2. Reaction-diffusion in the interior of a deforming surface. Within Ω, we solve the convection-reaction-diffusion of concentrations c_v with velocity fields $\mathbf{v}_v$, diffusion constants D_v, reaction terms $R_v(\mathbf{c}_v)$, and boundary condition terms $B_v(\mathbf{c})$:

$$\begin{aligned} \frac{\partial c_v}{\partial t} + \nabla \cdot (c_v \mathbf{v}_v) &= \nabla \cdot (D_v \nabla c_v) + R_v(\mathbf{c}_v) && \text{in } \Omega, \\ D_v \nabla c_v \cdot \mathbf{n} &= B_v(\mathbf{c}) && \text{on } \Gamma = \partial\Omega, \end{aligned} \tag{2.3}$$

where $\mathbf{n}$ is the outward pointing surface normal on Γ. We specify the velocity field $\mathbf{v}$ for volume species v and surface species s such that $\mathbf{v}_v = \mathbf{v}$ and $\mathbf{v}_\Gamma = \mathbf{v}|_\Gamma$. We note that the reaction terms $R_v(\mathbf{c}_v)$ can only depend on volume species. The boundary condition terms $B_v(\mathbf{c})$ can depend on both volume and surface species. As an example we consider coupling surface and volume concentrations by defining a transfer rate k_s for a surface species s to become a volume species v and a transfer rate α_v for the opposite direction. This is solved by defining a Robin boundary condition of the form $B_v(\mathbf{c}) = k_s c_s - \alpha_v c_v$ in (2.3) and reaction terms $R_s(\mathbf{c}) = -B_v(\mathbf{c})$ in (2.2).

2.3. Coupling reaction-diffusion in the interior and on the surface. We want to solve systems where the surface and volume concentrations can be coupled via boundary condition terms $B_v(\mathbf{c})$ and reaction terms $R_s(\mathbf{c})$ on arbitrarily deforming surfaces Γ. For that purpose, we immerse Ω in a larger computational domain D where we also define $\Omega_e = D \setminus \Omega$ and $\Gamma_e = \partial\Omega_e$ (see Figure 2.1). We then extend c_s and c_v into quantities $\tilde{c}_s$ and $\tilde{c}_v$ defined throughout the extended domain D such that

$$\begin{aligned} \tilde{c}_s|_\Gamma &\approx c_s, \\ \tilde{c}_v|_\Omega &\approx c_v. \end{aligned} \tag{2.4}$$

The extended representation also applies to the remaining space-dependent quantities $\mathbf{v}$, $\mathbf{c}$, $\mathbf{c}_v$ and D_v that appear in (2.2)–(2.3) which become $\tilde{\mathbf{v}}$, $\tilde{\mathbf{c}}$, $\tilde{\mathbf{c}}_v$, and $\tilde{D}_v$ in the extended domain D.

The surface Γ is represented as the zero isocontour of a level set function [37]:

$$\Gamma(t) = \{\mathbf{x}(t) \,|\, \phi(\mathbf{x}(t)) = 0\}. \tag{2.5}$$

The level set function is initialized as a signed distance function such that $|\nabla\phi| = 1$ and we define ϕ to be negative in Ω and positive on the outside. The outward pointing surface normal is computed as

$$\mathbf{n} = \nabla\phi / |\nabla\phi|. \tag{2.6}$$

We wish to solve an extended version of (2.2)–(2.3) in the shared computational domain D using the implicit surface representation given in (2.5). This will result in a set of equations coupling surface and volume concentrations without any splitting between surface and volume related events. Furthermore, the level set representation enables numerical simulations that can accurately capture large deformations. In the following, we describe the governing equations for the evolution of the level set function ϕ and the concentrations $\tilde{c}_s$ and $\tilde{c}_v$ in the domain D.

We solve (2.1) by varying the level set in time as governed by

$$\frac{\partial \phi}{\partial t} + \tilde{\mathbf{v}} \cdot \nabla\phi = 0, \tag{2.7}$$

where $\tilde{\mathbf{v}}$ can depend on various factors such as the concentration of a particular species.

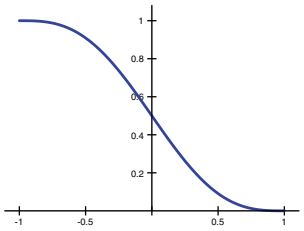

FIG. 2.2. *Phase field function* $\psi(\phi/w)$.

Following earlier work [6, 7], we extend the surface concentrations into a narrow band Γ_b around Γ with $|\phi| \leq \gamma$ (see Figure 2.1). Throughout this article, we choose $\gamma = 5\,h$, where h is the grid spacing. If we choose $\tilde{c}_s$ and the velocity field $\tilde{\mathbf{v}}$ such that

$$\frac{\partial \tilde{c}_s}{\partial \mathbf{n}} = 0 \text{ and } \frac{\partial\,(\mathbf{n}\cdot\tilde{\mathbf{v}})}{\partial \mathbf{n}} = 0, \tag{2.8}$$

we can rewrite (2.2) as

$$\frac{\partial \tilde{c}_s}{\partial t} + \nabla\cdot(\tilde{c}_s\tilde{\mathbf{v}}) = D_s\nabla\cdot((\mathbb{I}-\mathbf{n}\otimes\mathbf{n})\,\nabla\tilde{c}_s) + R_s(\tilde{\mathbf{c}}), \tag{2.9}$$

which can now be solved in the narrow band Γ_b.

We choose the phase field method to extend (2.3) into the computational domain D while using the implicit surface representation [22, 30]. We introduce the "phase field" ψ_w as a mollified Heaviside that is ≈ 1 inside Ω and ≈ 0 otherwise. We define ψ_w as a function of the level set ϕ with a width w ($\psi_w(\phi) = \psi(\phi/w)$) and we assume antisymmetry $\psi(x) = 1 - \psi(-x)$. In this work, we choose the function

$$\psi(x) = \begin{cases} 1, & x < -1, \\ \dfrac{1-x}{2} - \dfrac{\sin(\pi x)}{2\pi}, & -1 \leq x \leq 1, \\ 0, & x > 1 \end{cases} \tag{2.10}$$

with the properties $\psi(1) = 0$, $\psi(-1) = 1$, and $\psi'(-1) = \psi'(1) = 0$ (see Figure 2.2). We can now rewrite (2.3) as

$$\begin{aligned} \frac{\partial \tilde{c}_v}{\partial t} + \nabla\cdot(\tilde{c}_v\tilde{\mathbf{v}}) = \frac{\nabla\cdot(\psi_w\tilde{D}_v\nabla\tilde{c}_v)}{\psi_w} + R_v(\tilde{\mathbf{c}}_v) + B_v(\tilde{\mathbf{c}})\frac{(\psi_w')^2}{K\psi_w} \quad &\text{in } D, \\ \text{suitable boundary condition for } \tilde{c}_v \quad &\text{on } \Gamma_e, \end{aligned} \tag{2.11}$$

where $K = \int_\Omega (\psi_w')^2/A$ is a normalization factor and A is the area of the interface Γ. Throughout this work, we use periodic boundary conditions on Γ_e.

In (2.11) the diffusion operator is now computed as $\nabla\cdot(\psi_w\tilde{D}_v\nabla\tilde{c}_v)/\psi_w$ which is only meaningful for $\phi \leq w$. The boundary condition on Γ has been replaced by the term $B_v(\tilde{\mathbf{c}})(\psi_w')^2/(K\psi_w)$ that is defined in the extended domain D. The shape of this term is shown in Figure 2.3 and we note that it is only nonzero close to the boundary Γ for $|\phi| < w$. Throughout this work, we choose $w = 2\,h < \gamma$, where h is the grid spacing and γ defines the width of the narrow band Γ_b. This choice of w ensures that the $B_v(\tilde{\mathbf{c}})$ function can involve both surface and volume concentrations. We can therefore use $B_v(\tilde{\mathbf{c}})$ in (2.11) to couple the volume diffusion to the concentrations on the surface. Similarly, we can use $R_s(\tilde{\mathbf{c}})$ in (2.9) while enforcing (2.8) to allow the volume concentrations to affect the ones on the surface.

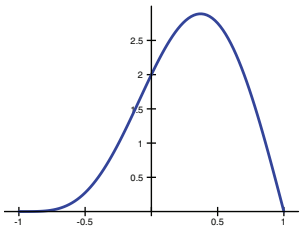

FIG. 2.3. *Boundary condition term* $(\psi')^2/\psi$.

3. Numerical method. We solve the governing equations (2.7), (2.9), (2.11) with a time splitting scheme. We first advance the system in time without advection as in

$$\frac{\partial \tilde{c}_s}{\partial t} = D_s \nabla \cdot \left((\mathbb{I} - \mathbf{n} \otimes \mathbf{n}) \nabla \tilde{c}_s \right) + R_s(\tilde{\mathbf{c}}), \tag{3.1}$$

$$\frac{\partial \tilde{c}_v}{\partial t} = \frac{\nabla \cdot (\psi_w \tilde{D}_v \nabla \tilde{c}_v)}{\psi_w} + R_v(\tilde{\mathbf{c}}_v) + B_v(\tilde{\mathbf{c}}) \frac{(\psi_w')^2}{K \psi_w}, \tag{3.2}$$

and then perform the advection part using a remeshed particle method to solve

$$\begin{aligned} \frac{\partial \phi}{\partial t} + \tilde{\mathbf{v}} \cdot \nabla \phi &= 0, \\ \frac{\partial \tilde{c}_s}{\partial t} + \nabla \cdot (\tilde{c}_s \tilde{\mathbf{v}}) &= 0, \\ \frac{\partial \tilde{c}_v}{\partial t} + \nabla \cdot (\tilde{c}_v \tilde{\mathbf{v}}) &= 0. \end{aligned} \tag{3.3}$$

The computational domain D is discretized on a regular lattice with grid spacing h. Summarizing, we initialize the fields $\tilde{\mathbf{c}}^0$ and ϕ^0 on the grid and then perform the following steps to compute the numerical solution of $\tilde{\mathbf{c}}^{n+1}$ and ϕ^{n+1} at time $t^{n+1} = t^n + \delta t$ given the solution $\tilde{\mathbf{c}}^n$ and ϕ^n at time t^n:

(i) *occasionally extend* $\tilde{c}_s^n$ *into the narrow band* Γ_b *for each species* s*;*
(ii) *compute reaction and diffusion terms on the surface and its interior;*
(iii) *perform time integration without the advection part to update* $\tilde{\mathbf{c}}^n \to \tilde{\mathbf{c}}'$*;*
(iv) *compute the velocity field* $\tilde{\mathbf{v}}$ *from* $\tilde{\mathbf{c}}'$ *and* ϕ^n*;*
(v) *generate particles carrying weights from the fields* $\tilde{\mathbf{c}}'$ *and* ϕ^n*;*
(vi) *move particles according to the velocity field* $\tilde{\mathbf{v}}$*;*
(vii) *interpolate particles back onto the regular lattice* $\to \tilde{\mathbf{c}}^{n+1}$ *and* ϕ^{n+1}*;*
(viii) *periodically reinitialize the level set function* ϕ^{n+1}*.*

A more detailed description of these steps is given in the next three subsections. The numerical method is implemented using the PPM library [44].

3.1. Reaction and diffusion terms on the surface. We solve (3.1) following the approach described in [6, 7]. First, we need to ensure that the property $\partial \tilde{c}_s / \partial \mathbf{n} = 0$ is kept. We therefore occasionally extend $\tilde{c}_s$ into Γ_b by solving the following PDE to steady state while keeping $\tilde{c}_s$ of the points with $|\phi| < h$ fixed [36, 40]:

$$\frac{\partial \tilde{c}_s}{\partial \tau} + sign(\phi) \nabla \phi \cdot \nabla \tilde{c}_s = 0. \tag{3.4}$$

We solve (3.4) with a weighted essentially nonoscillatory (WENO) scheme [19] and only update values within the narrow band Γ_b. A high order scheme is required

here since an $O(h^p)$ error in solving (3.4) leads to an $O(h^{p-2})$ error in the diffusion equation. The frequency of extensions depends on the width of the narrow band and the numerical scheme chosen to solve (3.1). Unless otherwise noted, we choose to extend every five time steps. A similar extension could also be performed for the velocity field $\tilde{\mathbf{v}}$ to conform to (2.8). Here, we will instead compute $\tilde{\mathbf{v}}$ as a function of the extended $\tilde{c}_s$. Furthermore, we avoid discontinuities in the velocity field by smoothly letting the velocity go to zero at the borders of Γ_b.

At this stage of the time step, all quantities are defined on a regular lattice and we use a second order finite difference stencil to discretize the anisotropic diffusion operator in (3.1). For a surface embedded in three dimensional space, the time step for time integration with forward Euler is limited by $\delta t < \frac{h^2}{6D_s}$ due to diffusion.

3.2. Reaction and diffusion terms in the interior of the surface. When solving (3.2), we can ignore points in Ω_e with $\phi > w$, where ϕ is the distance to the surface and w defines the width of the phase field. Following earlier work, we set $\partial\tilde{c}_v/\partial t = 0$ for $\psi_w < 10^{-8}$ [22]. Any space dependent variable in Ω needs to be extended into the region of Ω_e with $\phi \leq w$. We choose $\tilde{D}_v$ as an extension of D_v which is constant along the normal direction into Ω_e. The initial condition for $\tilde{\mathbf{c}}_v$ in Ω_e is set such that it is locally symmetric around the boundary Γ to minimize the error [22]. The constant $K = \int_\Omega (\psi'_w)^2/A$ in (3.2) could be computed numerically according to the discretization of the geometry but here we will use the value $K = \frac{3}{4w}$. This is valid if the maximal curvature is $\ll 1/h$.

Inhomogeneous diffusion of the form $\nabla \cdot (a\nabla c)$ as in (3.2) is discretized at each grid point i using a second order finite difference scheme:

$$\nabla \cdot (a\nabla c_i) \approx \frac{1}{h^2} \sum_{j \in N(i)} a_{i,j}\,(c_j - c_i), \tag{3.5}$$

where $N(i)$ is the set of neighbors of i. $a_{i,j}$ is computed using a harmonic mean [34]:

$$a_{i,j} = 2\left(\frac{1}{a_i} + \frac{1}{a_j}\right)^{-1} = \frac{2a_i a_j}{a_i + a_j}. \tag{3.6}$$

For the diffusion part, the time step for time integration with forward Euler is limited by $\delta t < \frac{h^2}{2d\tilde{D}_v}$, where d is the dimensionality of the problem. The reaction and boundary condition terms may additionally limit the time step. For example for a mass transport from the surface to the volume and vice versa, we have boundary condition terms of the form $B_v(\mathbf{c}) = k_s c_s - \alpha_v c_v$. This limits the time step as $\delta t < 1/\alpha_m$, where $\alpha_m \approx 3.9\,\alpha_v/w$ is the maximal value of $\alpha_v \frac{(\psi'_w)^2}{K\psi_w}$.

3.3. Advection using the remeshed particle method. The advection equations in (3.3) are solved using the remeshed particle method described in [6]. A scalar function $c(\mathbf{x}, t)$ can be represented as a superposition of particles with particle weights $c_p(t)$ located at positions $\mathbf{x}_p(t)$:

$$c(\mathbf{x}, t) = \sum_p c_p(t)\, J_\epsilon(\mathbf{x} - \mathbf{x}_p(t)), \tag{3.7}$$

where $J_\epsilon(\mathbf{x}) = \epsilon^{-d}\, J(\|\mathbf{x}\|/\epsilon)$ is the particle kernel function and d is the dimensionality of the problem. $J(i)$ has the Kronecker delta property $J(i) = \delta_{0i}$ and conserves the

first r moments according to

$$\int J(x)\, x^{\alpha}\, dx = 0^{\alpha}, \quad 0 \leq \alpha < r. \tag{3.8}$$

At this stage of the time step, we have the vector of concentrations $\tilde{\mathbf{c}}'$, the level set function ϕ^n, and the velocity field $\tilde{\mathbf{v}}$ defined on the grid. The contributions from the reaction and diffusion terms have already been added to $\tilde{\mathbf{c}}'$. We generate particles at the location of the grid points with weights $\mathbf{c}_p$ and ϕ_p to represent the fields $\tilde{\mathbf{c}}'$ and ϕ^n according to (3.7). We then move the particles by solving

$$\frac{d\mathbf{x}_p}{dt} = \tilde{\mathbf{v}}(\mathbf{x}_p, t) \tag{3.9}$$

for a single time step of size δt. Finally, we "remesh" the particles to deal with Lagrangian distortion and to allow for an efficient computation of the diffusion for the next time step [25]. For the concentrations $\mathbf{c}_p$ we can perform the remeshing by evaluating

$$\mathbf{c}_p^{new} = \sum_{p'} \mathbf{c}_p\, M_h(\mathbf{x}_{p'} - \mathbf{x}_p^{new}), \tag{3.10}$$

where $x_p^{new} = \mathbf{i}\, h$ are the new particle locations on the grid points and $M_h(\mathbf{x}) = M(\mathbf{x}/h)$ is the remeshing kernel. In this work, $M(\mathbf{x})$ is defined as the tensorial product of M_4' kernels. This choice of $M(\mathbf{x})$ conserves the first four moments of the field interpolated between particles and grid [25].

The situation is different for the level set function ϕ as it is subject to a nonconservative advection equation. We use Shepard's rule in order to maintain the property of partition of unity [46]:

$$\phi_p^{new} = \frac{\sum_{p'} \phi_p\, M_h(\mathbf{x}_{p'} - \mathbf{x}_p^{new})}{\sum_{p'} M_h(\mathbf{x}_{p'} - \mathbf{x}_p^{new})}. \tag{3.11}$$

As the level set function ϕ is advected, it loses the property that $|\nabla\phi| = 1$, i.e., it is no longer a signed distance function. Therefore, we periodically reinitialize the level set so that it maintains this property by solving

$$\frac{\partial\phi}{\partial\tau} + sign(\phi_o)\,(|\nabla\phi| - 1) = 0 \tag{3.12}$$

to steady state, where $\phi_o = \phi(\tau = 0)$ [36]. We solve (3.12) with a WENO scheme [19]. The frequency of reinitialization is controlled by measuring the furthest distance a particle has moved and sum over consecutive time steps until we have surpassed $c_{reinit}h$, where c_{reinit} is the reinitialization parameter. This ensures that the difference between ϕ and the actual signed distance to Γ will converge as the grid is refined. Unless otherwise noted, we choose $c_{reinit} = 0.45$.

3.4. Geometric constraints. To investigate the effect of geometric constraints, we allow the velocity field $\tilde{\mathbf{v}}$ to be limited by an obstructing surface Γ_o as shown in

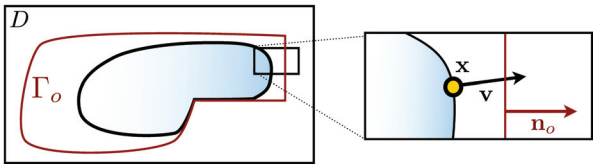

FIG. 3.1. *Sketch of deforming surface close to an obstructing surface* Γ_o.

Figure 3.1. We use a signed distance function ϕ_o to represent geometries of arbitrary shape and to compute their surface normal $\mathbf{n}_o$. We then update the velocity field as

$$\tilde{\mathbf{v}}^{new} = \tilde{\mathbf{v}} - \psi(-\phi_o/w_o - 1)\,(\mathbf{n}_o \cdot \tilde{\mathbf{v}})\,\mathbf{n}_o, \tag{3.13}$$

where $\psi(x)$ is the mollified Heaviside defined in (2.10) and w_o is the mollification width which we set to $w_o = 2\,h$.

3.5. Boundary conditions on edges of the surface. We wish to model reaction-diffusion systems on nonclosed surfaces like the hemisphere surface. This requires boundary conditions to be defined on the boundary of the surface. Here, we only consider boundaries which we can define by cutting a closed surface by a plane. We can then compute "ghost values" outside of Γ_b on the other side of the plane according to a Taylor expansion to enforce the boundary condition.

4. Results. In this section we show results from the application of our method to benchmark problems for reaction-diffusion equations. Furthermore, we present results for pattern-forming reaction-diffusion systems with deforming domains. In section 4.1, we consider a reaction-diffusion system on a deforming surface, compare with published results and extend the system to include geometric constraints. We then assess the accuracy of the phase-field method for reaction-diffusion inside a volume in section 4.2. The accuracy of our approach to couple reaction-diffusion on a deforming surface and its interior is compared with published results in section 4.3. In section 4.4, we demonstrate our approach on a pattern-forming Schnakenberg model.

4.1. Reaction-diffusion on a deforming surface with the Brusselator. We compare our method for reaction-diffusion on a deforming surface with an alternative method using a triangulated surface [16]. Furthermore, we wish to check our proposed method for boundary conditions on edges of the surface and we wish to examine the effect of geometric constraint on the deforming surface.

A variant of the Brusselator reaction-diffusion system was proposed as a patterning mechanism for plant growth [16]. The system defines the evolution of two species X and Y diffusing along a surface and reacting with each other. It is known to produce stable patterns on a static surface. The initial geometry is a hemisphere where the surface boundary is subject to a no-flux boundary condition and is not allowed to move. The velocity field is oriented in the direction of the surface normal and is proportional to X. X and Y evolve according to

$$\begin{aligned}
\frac{\partial X}{\partial t} + \nabla_\Gamma \cdot (X\mathbf{v}) &= \begin{cases} D_X \Delta_\Gamma X + aA - bBX + cX^2Y - dX & \text{if } X > X_{th}, \\ D_X \Delta_\Gamma X - dX & \text{if } X \le X_{th} \end{cases} \\
\frac{\partial Y}{\partial t} + \nabla_\Gamma \cdot (Y\mathbf{v}) &= \begin{cases} D_Y \Delta_\Gamma Y + bBX - cX^2Y & \text{if } X > X_{th}, \\ D_Y \Delta_\Gamma Y & \text{if } X \le X_{th}, \end{cases} \\
X_0 = X(t=0) = \frac{aA}{d},\ Y_0 &= Y(t=0) = \frac{bB}{cX_0}.
\end{aligned} \tag{4.1}$$

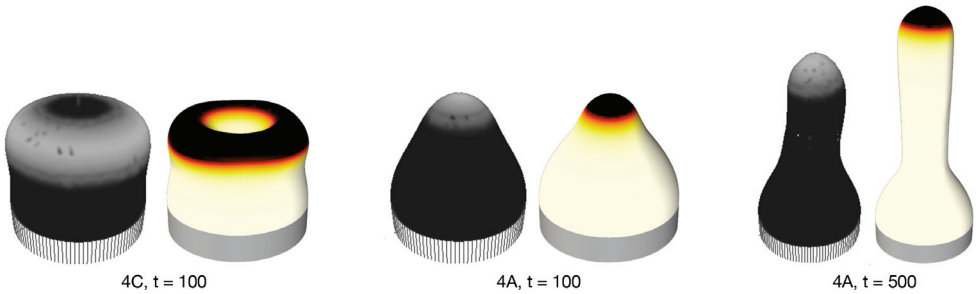

FIG. 4.1. *Comparison with software provided by* [16]. *On the surface we visualize their results (grayscale with black values being low) compared with our results (white (low) to black (high)) for species* X. *The results labeled "4C" use the default set of parameters explained in the text. The results labeled "4A" use parameters as in Figure 4A of* [16] *with* $A = 1 + 10\,Y_1^0$ *and* $D_X = 0.025$.

The velocity field $\mathbf{v}$ is computed as

$$\mathbf{v} = v\,\eta(|\phi|)\,X\,\mathbf{n},$$

$$\eta(|\phi|) = \begin{cases} 1, & |\phi| < 2h, \\ \dfrac{(|\phi| - h)\,(|\phi| - 4h)^2}{4h^3}, & 2h \le |\phi| < 4h, \\ 0, & |\phi| \ge 4h, \end{cases} \tag{4.2}$$

where $\eta(|\phi|)$ uses the level set function ϕ to smoothly let the velocity go to zero at the borders of Γ_b. Our default set of parameters is chosen according to Figure 4C of [16]. The parameters are $D_X = 0.012$, $D_Y = 20\,D_X$, $a = 0.01$, $bB = 1.5$, $c = 1.8$, $d = 0.07$, $X_{th} = 0.035$, and $A = 1 + 30\,Y_1^0$, where Y_1^0 is the (1,0) spherical harmonic. The velocity is scaled with $v = 0.00125$ and we let the pattern evolve without deformation until $t = 10$.

Figure 4.1 shows a comparison of our results with results produced using the software provided by [16]. Their method represents the surface explicitly with finite elements. This has the advantage of having one computational element per surface element while in our method we have many in the narrow band. The main expected disadvantage is a large computational cost to remesh the surface for large deformations or, alternatively, a lack of robustness in those cases. In [16], it is mentioned that their code loses accuracy in concave regions. When running their software, we noticed that it tends to keep the surface convex and this effect is visible in the leftmost figures of Figure 4.1. In the rightmost figures of Figure 4.1 one can see random growth directions in their result. In their method, the surface is deformed by visiting the finite elements in random order and moving them in a normal direction until the area has been increased by a factor proportional to the concentration of the surface species. Our method does not have these artificial fluctuations.

Figure 4.2 illustrates the robustness of the method with respect to large changes in the geometry. While the surface deforms, the reaction-diffusion system continuously changes the pattern which can lead to significantly different shapes.

Figure 4.3 shows the effect of adding geometric constraints to the system. We run the system with the same default set of parameters as before but limit the growth by a box. In this case, the constraint does not seem to have a major effect on the pattern as compared with Figure 4.2.

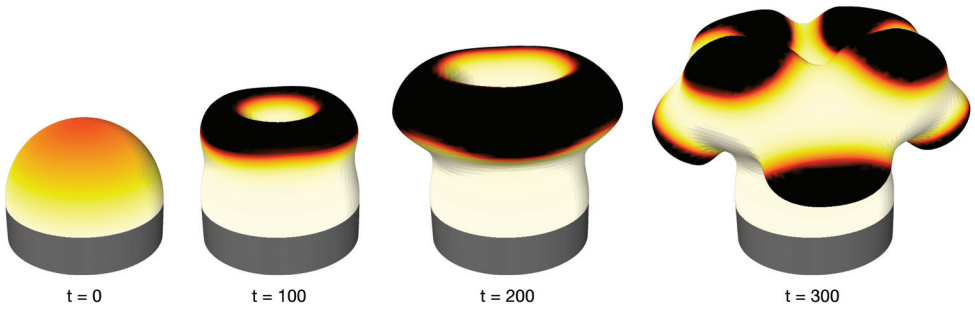

FIG. 4.2. *Long run using settings as in Figure* 4*C of* [16]. *The color of the surface shows the species X as in Figure* 4.1 *(white (low) to black (high)) (the image was adapted from* [26]*).*

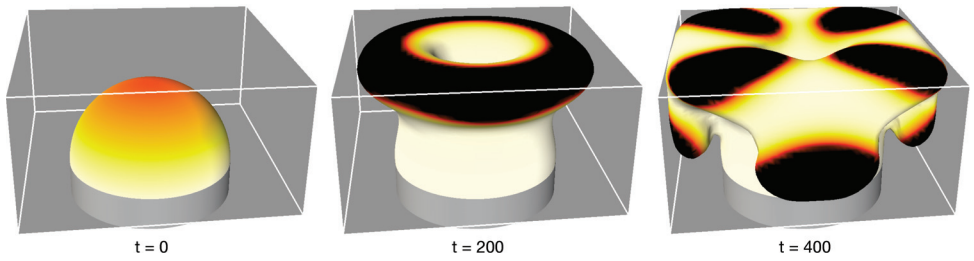

FIG. 4.3. *Same system as in Figure* 4.2 *but with growth limited by a box.*

4.2. Accuracy of reaction-diffusion inside a volume. Before coupling surface and volume diffusion, we assess the accuracy of our method for volume diffusion only. We consider the concentration c_v in a 2D, circular domain Ω with radius R and solve

$$\begin{aligned} \frac{\partial c_v}{\partial t} &= D_v \Delta c_v, && \text{in } \Omega, \\ \alpha_v c_v + D_v \nabla c_v \cdot \mathbf{n} &= \frac{\alpha_v \left(4aD_v t + 1\right) - 2aD_v R}{\pi \left(4aD_v t + 1\right)^2} \exp\left(-\frac{aR^2}{4aD_v t + 1}\right) && \text{on } \Gamma, \end{aligned} \tag{4.3}$$

which has the following exact solution in polar coordinates:

$$c_v(r, \theta, t) = \frac{1}{\pi \left(4aD_v t + 1\right)} \exp\left(-\frac{ar^2}{4aD_v t + 1}\right). \tag{4.4}$$

We choose $R = 0.25$, $a = 10$, $D_v = 0.005$, and run up to $t = 10$. Furthermore, we use a forward Euler time integration and choose the time step according to

$$\delta t = \min\left(\frac{h^2}{8D_v}, \frac{h}{3\alpha_v}\right). \tag{4.5}$$

Given the computed numerical solutions c_i at each grid point i within Ω and the exact analytical result c_e at $t = 10$, we compute the $L_\infty = \max_i(|c_i - c_e|)$ as well as the L_1 and L_2 norms defined as

$$L_p = \left(\frac{\sum_i |c_i - c_e|^p \, vol_i}{\sum_i vol_i}\right)^{1/p}, \tag{4.6}$$

where vol_i is the volume of the ith grid point. Convergence for nonzero Neumann boundary conditions ($\alpha_v = 0$) and Robin boundary conditions ($\alpha_v \neq 0$) are shown in

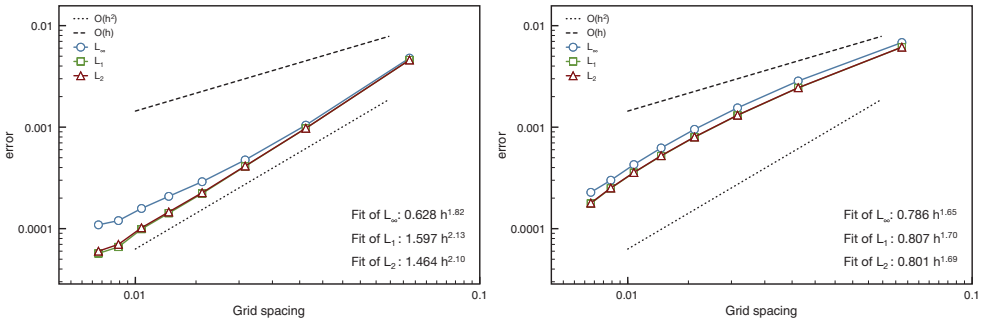

FIG. 4.4. *Convergence for exponential test case with Neumann boundary condition (left, $\alpha_v = 0$) and Robin boundary condition (right, $\alpha_v = 1$).*

Figure 4.4. With Neumann boundary conditions we achieve a convergence rate close to second order. Robin boundary conditions, on the other hand, lead to a slightly increased error and worse convergence rate at low resolutions. We believe that the reason for the increased error is that in (2.11) we use $\alpha_v \tilde{c}_v$ to enforce the Robin boundary condition while we should use $\alpha_v \tilde{c}_v|_\Gamma$ at the closest point on Γ.

4.3. Accuracy of coupled reaction-diffusion on a surface and its interior. In order to assess the accuracy of the proposed coupling between surface and volume diffusion, we solve the following system involving the concentration c_v in the volume Ω and the concentration c_s on the surface Γ [35]:

$$\begin{aligned} \frac{\partial c_s}{\partial t} &= \Delta_\Gamma c_s + c_v - c_s && \text{on } \Gamma, \\ \frac{\partial c_v}{\partial t} &= \Delta c_v && \text{in } \Omega, \\ \nabla c_v \cdot \mathbf{n} &= c_s - c_v && \text{on } \Gamma, \end{aligned} \tag{4.7}$$

where Ω is the unit sphere. The exact solution in spherical coordinates is given by

$$\begin{aligned} c_s(\theta, \varphi, t) &= A \exp(-k^2 t) \cos(\theta), \\ c_v(r, \theta, \varphi, t) &= \exp(-k^2 t) \cos(\theta) \left(\frac{\sin(kr)}{k^2 r^2} - \frac{\cos(kr)}{kr} \right), \\ A &= \sin(k) + \frac{\cos(k)}{k} - \frac{\sin(k)}{k^2}, \end{aligned} \tag{4.8}$$

where $k = 1.527338738393456$ was computed numerically. The system is solved up to $t = 0.1$. The same norms as in section 4.2 are computed for the relative error of the solution of c_s which we approximate as the values of $\tilde{c}_s$ with $|\phi| < h$.

Figure 4.5 shows the results of the refinement study compared with published results [35]. We note that while the L_∞ error converges close to the $O(h^{1.4})$ reported by Novak, the L_1 and L_2 errors converge close to second error.

4.4. Reaction-diffusion on a deforming surface and its interior. The Schnakenberg system was proposed as a prepatterning system in tumor growth [9]. Similarly to the Brusselator system, we have two species X and Y diffusing and reacting on a surface. It is also known to generate steady patterns on static geometries. Here, we introduce an additional species Z representing a variant of X which can freely

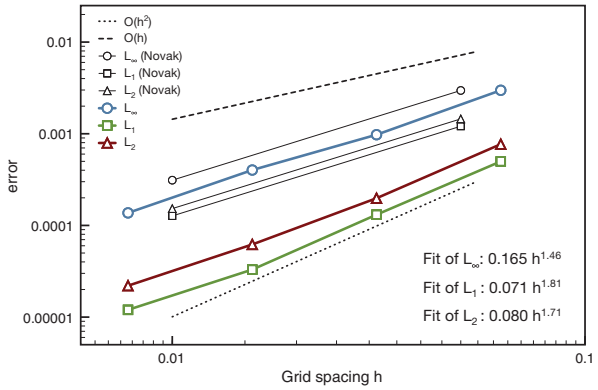

FIG. 4.5. *Convergence for coupled system on sphere and in volume compared to results reported by Novak et al.* [35].

diffuse within the interior of the surface. X, Y, and Z evolve according to

$$
\begin{aligned}
&\frac{\partial X}{\partial t} + \nabla_\Gamma \cdot (X\mathbf{v}) = D_X \Delta_\Gamma X + aX^2Y + b - cX + \alpha Z - kX && \text{on } \Gamma,\\
&\frac{\partial Y}{\partial t} + \nabla_\Gamma \cdot (Y\mathbf{v}) = D_Y \Delta_\Gamma Y - aX^2Y + d && \text{on } \Gamma,\\
&\frac{\partial Z}{\partial t} + \nabla \cdot (Z\mathbf{v}) = D_Z \Delta Z && \text{in } \Omega,\\
&D_Z \nabla Z \cdot \mathbf{n} = kX - \alpha Z && \text{on } \Gamma,
\end{aligned}
\tag{4.9}
$$

where k and α control the transfer rates from X to Z and vice versa. The initial conditions are set to

$$
X(t=0) = \frac{b+d}{c}R, \quad Y(t=0) = \frac{c^2 d}{a\,(b+d)^2}R, \quad Z(t=0) = \frac{k\,(b+d)}{\alpha c},
\tag{4.10}
$$

where $R \sim \mathcal{U}(0.995, 1.005)$ adds random noise to the homogenous steady state solution of (4.9). For the surface species we use the parameters of "Experiment 4" in [9]: $D_X = 1$, $D_Y = 25$, $a = 100$, $b = 20$, $c = 100$, and $d = 100$. For the volume species Z we choose $D_Z = 1$ and consider the transfer rates $k = \alpha = 10$ and $k = \alpha = 100$.

The velocity field $\mathbf{v}$ is computed as

$$
\begin{aligned}
&\mathbf{v} = v\,(\,\eta(|\phi|)\,v_s + (1-\eta(|\phi|))\,v_v)\,\mathbf{n},\\
&v_s = X - \frac{b+d}{c},\\
&v_v = \begin{cases} \dfrac{\alpha Z + D_Z \nabla Z \cdot \mathbf{n}}{k} - \dfrac{b+d}{c}, & \phi \le 0,\\ 0, & \phi > 0, \end{cases}
\end{aligned}
\tag{4.11}
$$

where $\eta(|\phi|)$ is the same function that was used in section 4.1 to smoothly let the velocity go to zero at the borders of Γ_b. We note that v_v was chosen such that $v_v = v_s$ on the surface Γ while $\eta(|\phi|)$ ensures a smooth transition between v_v and v_s. The velocity is scaled by $v = 0.05$ and we let the pattern evolve without deformation until $t = 5$. Without diffusion in the volume, we set $k = \alpha = v_v = 0$, drop Z, and solve the system only on the surface.

At approximately $t = 5$, the system reaches a stable pattern of spots on a sphere (see top left image in Figure 4.6). Similar patterns are observed when we couple it to

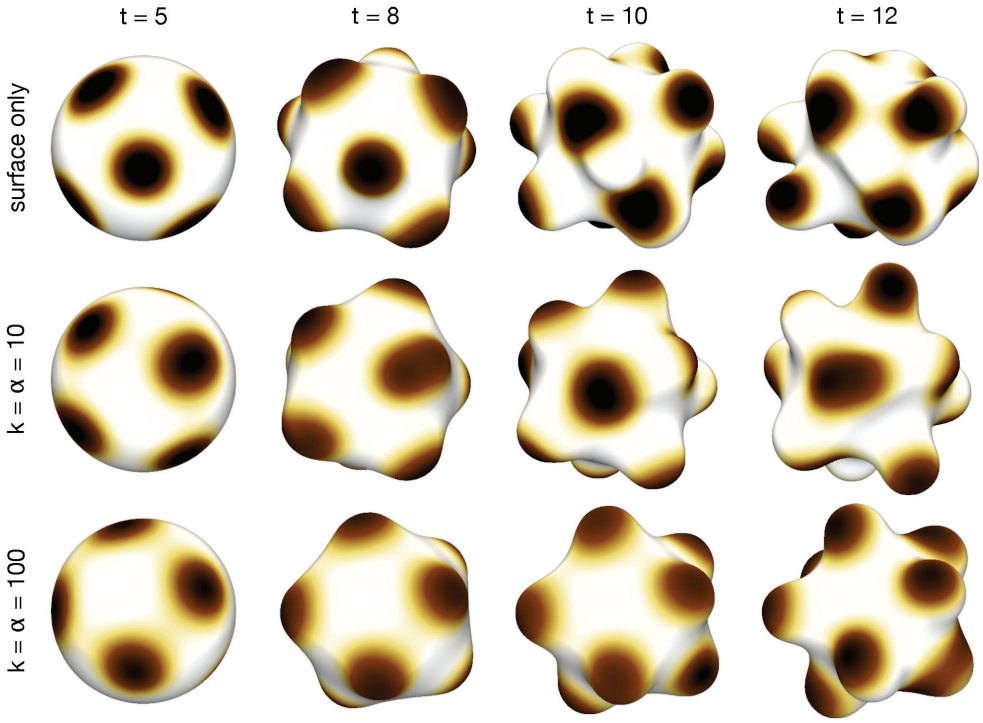

FIG. 4.6. *Growing Schnakenberg system on surface and with coupled volume diffusion. From left to right we see the evolution of the surface. On the surface the concentration X is shown (black is high, white is low). The rows represent systems without volume diffusion and with volume diffusion coupled by transfer rates $k = \alpha = 10$ and $k = \alpha = 100$.*

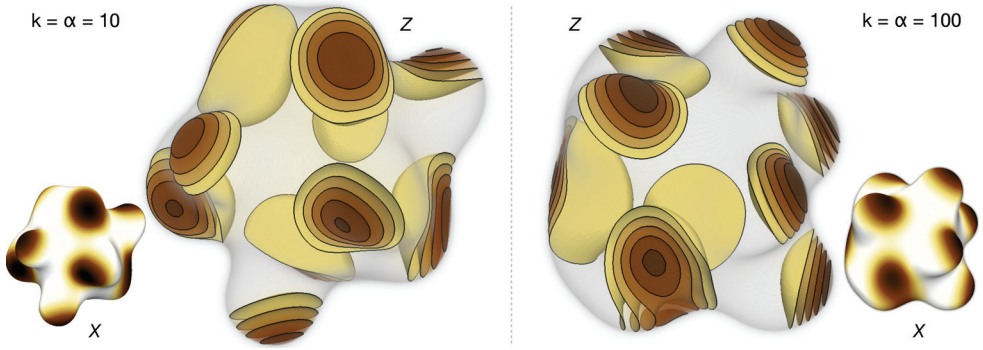

FIG. 4.7. *Isocontours of volume concentration Z at $t = 12$ for Schnakenberg system with volume diffusion coupled by transfer rates $k = \alpha = 10$ (left) and $k = \alpha = 100$ (right). The smaller images show the surface concentration X. The same colormap as in* Figure 4.6 *is used.*

diffusion within the volume (see first column in Figure 4.6). After $t = 5$, we introduce the velocity field and observe that the pattern of spots on the surface remains more stable as k and α are increased (see Figure 4.6).

The volume concentration Z at $t = 12$ is shown in Figure 4.7. We can see that the pattern of Z closely follows the one of X keeping $\nabla Z \cdot \mathbf{n}$ close to 0 on the surface.

Z can then accelerate the diffusive transport of X by taking a shortcut through the volume in convex regions such as the "spikes" that form while growing.

5. Conclusions. We combine remeshed particles with phase field models, to simulate, for the first time, reaction-diffusion equations in the volume and on the surface of deforming geometries. A remeshed particle method is used to discretize the level set equations that define the deforming surfaces. The remeshed particles are combined with a phase field method so as to enforce boundary conditions that enable the coupling of the evolution of substances in the volume and the lumen. The method allows for nonclosed surfaces like the hemisphere surface and the study of geometric constraints limiting the growth. The accuracy of the method is demonstrated on benchmark problems and by comparison with published results. We show that the method can handle arbitrarily deformed geometries that occur when the surface velocity depends on the pattern formed by a Turing-like reaction-diffusion system.

The simulation of diffusion on the surface relies on an implicit representation of the surface and as such it requires more computational elements compared to an explicit representation. On the other hand, this representation allows for simpler and more regular operations on those computational elements, a feature that can be exploited for the efficient parallelization and vectorization of the implementation. Another potential drawback of the method can be the need to frequently solve (3.4) to steady state within the narrow band Γ_b. The benefits of not having to retriangulate the surface can compensate for this drawback.

For systems with coupled reaction-diffusion equations, the computational cost of the proposed method, for the spatial discretizations, is $O(N)$, where N is the number of particles. Future work will focus on the development of multiresolution remeshed particle and phase field methods for the solution of reaction-diffusion equations, allowing for a more efficient use of the computational elements.

We note that the proposed method can be extended to surface-volume interactions beyond reaction-diffusion. Of particular interest are systems where surface species affect the mechanical properties of the boundary of an elastic solid [15] or tumor growth where diffusing volume species affect surface reactions rates [8, 32].

Appendix A. Comparison of methods to solve PDEs with irregular boundaries. Several methods have been proposed to solve PDEs within irregular and deforming geometries or where such a geometry is immersed in a larger domain. In both cases one could use a body fitted mesh and solve the system with an FEM [53], but this would require expensive remeshing when the geometry is deformed. In this section we compare methods that solve these kinds of PDEs without a body fitted mesh, but where the surface is given implicitly (e.g., with a level set function).

Table A.1 compares a selection of methods that may be suited to solve PDEs within irregular and deforming geometries. In this work we wish to accurately solve a parabolic PDE (the diffusion equation) with Robin boundary conditions. We also wish to couple the method with quantities diffusing on the surface according to (2.9) which is solved in the narrow band Γ_b. It is therefore desirable to have access to volume quantities within a similar narrow band. We note that methods suited to solve PDEs with an immersed geometry or with discontinuous coefficients may not generally be suited to solve diffusion equations within irregular and deforming geometries with Robin boundary conditions as in (2.3). To the best of our knowledge there is no immersed interface method that could solve such an equation. Under these considerations, the phase field method of Levine and Rappel [30] is best suited for our problem. We note that the level set method proposed by Papac et al. [38] could also

TABLE A.1

Comparison of methods to solve PDEs with irregular boundaries. Types of PDEs solved: Parabolic PDE (e.g., diffusion equation) (P), Elliptic PDE (e.g., Poisson's equation) (E), Navier–Stokes equation (NS). Accuracy is given as the approximate convergence in space for benchmark problems as reported in the given reference. Cost refers to the expected computational cost. Types of supported boundary conditions (BC): Robin BC (RBC), Neumann BC (NBC), Dirichlet BC (DBC), immersed interfaces (II). Methods are marked with an "X" in the last column if the data is also defined in a narrow band (NB).

Method & Citation	PDE	Accuracy	Cost	Supported BC	NB
Phase field [22]	P	2nd*	low	NBC	X
Phase field [30]	P	2nd*	low	RBC, NBC	X
Interface penalization [42]	E	1st	low	RBC, NBC, DBC	X
Volume penalization [20]	P	$<$ 1st	low	NBC	X
Level set with extrapolation [38]	P, E	2nd	high	RBC, NBC	X
Cut-cell finite volume [48]	P	2nd	medium	RBC, NBC	
Virtual node [4]	E	2nd	low	NBC, DBC, II	
Immersed boundary [41]	NS	1st	low	II	X
Immersed interface [29]	E	2nd	low	II	X
Level set [12]	P, E	2nd	low	DBC, II	X
Immersed finite element [17]	E	2nd	low	II	X

* shown within this work

have been considered but it has a considerably higher computational cost to enforce the boundary condition. The method they use to enforce Robin boundary conditions requires the solution of three equations like (3.4) to steady state in each time step. This is considerably more expensive than evaluating the term $B_v(\tilde{\mathbf{c}})(\psi_w')^2/(K\psi_w)$ in (2.11).

Acknowledgments. The authors thank M. Bergdorf for guidance at the start of the project, J. Halatek for pointing us to the phase field method for diffusion equations, and F. Milde for critical comments on the manuscript.

REFERENCES

[1] D. ADALSTEINSSON AND J. A. SETHIAN, *Transport and diffusion of material quantities on propagating interfaces via level set methods*, J. Comput. Phys., 185 (2003), pp. 271–288.

[2] R. E. BAKER AND P. K. MAINI, *A mechanism for morphogen-controlled domain growth*, J. Math. Biol., 54 (2007), pp. 597–622.

[3] R. A. BARRIO, C. VAREA, J. L. ARAGON, AND P. K. MAINI, *A two-dimensional numerical study of spatial pattern formation in interacting Turing systems*, Bull. Math. Biol., 61 (1999), pp. 483–505.

[4] J. BEDROSSIAN, J. H. VON BRECHT, S. ZHU, E. SIFAKIS, AND J. M. TERAN, *A second order virtual node method for elliptic problems with interfaces and irregular domains*, J. Comput. Phys., 229 (2010), pp. 6405–6426.

[5] M. BERGDORF AND P. KOUMOUTSAKOS, *A Lagrangian particle-wavelet method*, Multiscale Model. Simul., 5 (2006), pp. 980–995.

[6] M. BERGDORF, I. SBALZARINI, AND P. KOUMOUTSAKOS, *A Lagrangian particle method for reaction-diffusion systems on deforming surfaces*, J. Math. Biol., 61 (2010), pp. 649–663.

[7] M. BERTALMIO, L. T. CHENG, S. OSHER, AND G. SAPIRO, *Variational problems and partial differential equations on implicit surfaces*, J. Comput. Phys., 174 (2001), pp. 759–780.

[8] D. BRESCH, T. COLIN, E. GRENIER, B. RIBBA, AND O. SAUT, *Computational modeling of solid tumor growth: The avascular stage*, SIAM J. Sci. Comput., 32 (2010), pp. 2321–2344.

[9] M. A. J. Chaplain, M. Ganesh, and I. G. Graham, *Spatio-temporal pattern formation on spherical surfaces: Numerical simulation and application to solid tumour growth*, J. Math. Biol., 42 (2001), pp. 387–423.
[10] G.-H. Cottet and A. Magni, *TVD remeshing formulas for particle methods*, C. R. Math., 347 (2009), pp. 1367–1372.
[11] D. Enright, R. Fedkiw, J. Ferziger, and I. Mitchell, *A hybrid particle level set method for improved interface capturing*, J. Comput. Phys., 183 (2002), pp. 83–116.
[12] F. Gibou, R. Fedkiw, R. Caflisch, and S. Osher, *A level set approach for the numerical simulation of dendritic growth*, J. Sci. Comput., 19 (2003), pp. 183–199.
[13] J. Halatek and E. Frey, *Highly canalized MinD transfer and MinE sequestration explain the origin of robust MinCDE-protein dynamics*, Cell Rep., 1 (2012), pp. 741–52.
[14] S. E. Hieber and P. Koumoutsakos, *A Lagrangian particle level set method*, J. Comput. Phys., 210 (2005), pp. 342–367.
[15] S. E. Hieber and P. Koumoutsakos, *A Lagrangian particle method for the simulation of linear and nonlinear elastic models of soft tissue*, J. Comput. Phys., 227 (2008), pp. 9195–9215.
[16] D. M. Holloway and L. G. Harrison, *Pattern selection in plants: Coupling chemical dynamics to surface growth in three dimensions*, Ann. Botany, 101 (2008), pp. 361–374.
[17] S. Hou, Z. Li, L. Wang, and W. Wang, *A numerical method for solving elasticity equations with interfaces*, Comm. Comput. Phys., 12 (2012), pp. 595–612.
[18] J. Howard, S. W. Grill, and J. S. Bois, *Turing's next steps: The mechanochemical basis of morphogenesis*, Nature Rev. Molec. Cell Biol., 12 (2011), pp. 392–398.
[19] G.-S. Jiang and D. Peng, *Weighted ENO schemes for Hamilton–Jacobi equations*, SIAM J. Sci. Comput., 21 (2000), pp. 2126–2143.
[20] B. Kadoch, D. Kolomenskiy, P. Angot, and K. Schneider, *A volume penalization method for incompressible flows and scalar advection–diffusion with moving obstacles*, J. Comput. Phys., 231 (2012), pp. 4365–4383.
[21] A. J. Koch and H. Meinhardt, *Biological pattern formation: From basic mechanisms to complex structures*, Rev. Modern Phys., 66 (1994), pp. 1481–1507.
[22] J. Kockelkoren, H. Levine, and W. Rappel, *Computational approach for modeling intra- and extracellular dynamics*, Phys. Rev. E (3), 68 (2003), 037702.
[23] S. Kondo and T. Miura, *Reaction-diffusion model as a framework for understanding biological pattern formation*, Science, 329 (2010), pp. 1616–1620.
[24] P. Koumoutsakos, *Inviscid axisymmetrization of an elliptical vortex*, J. Comput. Phys., 138 (1997), pp. 821–857.
[25] P. Koumoutsakos, *Multiscale flow simulations using particles*, Annu. Rev. Fluid Mech., 37 (2005), pp. 457–487.
[26] P. Koumoutsakos, B. Bayati, F. Milde, and G. Tauriello, *Particle simulations of morphogenesis*, Math. Models Methods Appl. Sci., 21 (2011), pp. 955–1006.
[27] S. Leung, J. Lowengrub, and H. Zhao, *A grid based particle method for solving partial differential equations on evolving surfaces and modeling high order geometrical motion*, J. Comput. Phys., 230 (2011), pp. 2540–2561.
[28] S. Leung and H. Zhao, *A grid based particle method for moving interface problems*, J. Comput. Phys., 228 (2009), pp. 2993–3024.
[29] R. J. LeVeque and Z. Li, *The immersed interface method for elliptic equations with discontinuous coefficients and singular sources*, SIAM J. Numer. Anal., 31 (1994), pp. 1019–1044.
[30] H. Levine and W. Rappel, *Membrane-bound turing patterns*, Phys. Rev. E (3), 72 (2005), 061912.
[31] C. B. Macdonald and S. J. Ruuth, *The implicit closest point method for the numerical solution of partial differential equations on surfaces*, SIAM J. Sci. Comput., 31 (2010), pp. 4330–4350.
[32] P. Macklin, S. McDougall, A. A. Anderson, M. J. Chaplain, V. Cristini, and J. Lowengrub, *Multiscale modelling and nonlinear simulation of vascular tumour growth*, J. Math. Biol., 58 (2009), pp. 765–798.
[33] A. Madzvamuse and P. K. Maini, *Velocity-induced numerical solutions of reaction-diffusion systems on continuously growing domains*, J. Comput. Phys., 225 (2007), pp. 100–119.
[34] I. D. Mishev, *Finite volume methods on Voronoi meshes*, Numer. Methods Partial Differential Equations, 14 (1998), pp. 193–212.
[35] I. L. Novak, F. Gao, Y.-S. Choi, D. Resasco, J. C. Schaff, and B. M. Slepchenko, *Diffusion on a curved surface coupled to diffusion in the volume: Application to cell biology*, J. Comput. Phys., 226 (2007), pp. 1271–1290.
[36] S. Osher and R. P. Fedkiw, *Level Set Methods and Dynamic Implicit Surfaces*, Appl. Math. Sci. 133, Springer, New York, 2003.

[37] S. Osher and J. A. Sethian, *Fronts propagating with curvature-dependent speed: Algorithms based on Hamilton-Jacobi formulations*, J. Comput. Phys., 79 (1988), pp. 12–49.
[38] J. Papac, F. Gibou, and C. Ratsch, *Efficient symmetric discretization for the Poisson, heat and Stefan-type problems with Robin boundary conditions*, J. Comput. Phys., 229 (2010), pp. 875–889.
[39] J. E. Pearson, *Complex patterns in a simple system*, Science, 261 (1993), pp. 189–192.
[40] D. Peng, B. Merriman, S. Osher, H. Zhao, and M. Kang, *A PDE-based fast local level set method*, J. Comput. Phys., 155 (1999), pp. 410–438.
[41] C. S. Peskin, *Flow patterns around heart valves: A numerical method*, J. Comput. Phys., 10 (1972), pp. 252–271.
[42] I. Ramiere, P. Angot, and M. Belliard, *A fictitious domain approach with spread interface for elliptic problems with general boundary conditions*, Comput. Methods Appl. Mech. Engrg., 196 (2007), pp. 766–781.
[43] S. J. Ruuth and B. Merriman, *A simple embedding method for solving partial differential equations on surfaces*, J. Comput. Phys., 227 (2008), pp. 1943–1961.
[44] I. F. Sbalzarini, J. H. Walther, M. Bergdorf, S. E. Hieber, E. M. Kotsalis, and P. Koumoutsakos, *PPM - a highly efficient parallel particle-mesh library for the simulation of continuum systems*, J. Comput. Phys., 215 (2006), pp. 566–588.
[45] J. A. Sethian, *Level Set Methods and Fast Marching Methods*, 2nd ed., Cambridge University Press, Cambridge, 1999.
[46] D. Shepard, *A two-dimensional interpolation function for irregularly-spaced data*, in Proceedings of the 1968 23rd ACM National Conference, ACM, New York, 1968, pp. 517–524.
[47] J. Soriano, S. Rudiger, P. Pullarkat, and A. Ott, *Mechanogenetic coupling of hydra symmetry breaking and driven Turing instability model*, Biophys. J., 96 (2009), pp. 1649–1660.
[48] W. Strychalski, D. Adalsteinsson, and T. C. Elston, *Simulating biochemical signaling networks in complex moving geometries*, SIAM J. Sci. Comput., 32 (2010), pp. 3039–3070.
[49] D. W. Thompson, *On Growth and Form*, 2nd ed., Cambridge University Press, Cambridge, 1945.
[50] A. M. Turing, *The chemical basis of morphogenesis*, R. Soc. Lond. Philos. Trans. Ser. B Biol. Sci., 237 (1952), pp. 37–72.
[51] C. Varea, J. L. Aragon, and R. A. Barrio, *Turing patterns on a sphere*, Phys. Rev. E (3), 60 (1999), pp. 4588–4592.
[52] J. J. Xu and H. K. Zhao, *An Eulerian formulation for solving partial differential equations along a moving interface*, J. Sci. Comput., 19 (2003), pp. 573–594.
[53] O. C. Zienkiewicz, R. L. Taylor, and J. Z. Zhu, *The Finite Element Method: Its Basis and Fundamentals*, 6th ed., Elsevier Butterworth-Heinemann, Boston, 2005.